Gadolinium-Free Cardiac MRI Myocardial Scar Detection by 4D Convolution Factorization

Amine Amyar[1], Shiro Nakamori[1], Manuel Morales[1], Siyeop Yoon[1], Jennifer Rodriguez[1], Jiwon Kim[2], Robert M. Judd[3], Jonathan W. Weinsaft[2], and Reza Nezafat[1(✉)]

[1] Department of Medicine (Cardiovascular Division), Beth Israel Deaconess Medical Center and Harvard Medical School, Boston, MA, USA
rnezafat@bidmc.harvard.edu
[2] Division of Cardiology, Weill Cornell Medicine, New York, NY, USA
[3] Department of Medicine (Cardiology Division), Duke University, Durham, NC, USA

Abstract. Gadolinium-based contrast agents are commonly used in cardiac magnetic resonance (CMR) imaging to characterize myocardial scar tissue. Recent works using deep learning have shown the promise of contrast-free short-axis cine images to detect scars based on wall motion abnormalities (WMA) in ischemic patients. However, WMA can occur in patients without a scar. Moreover, the presence of a scar may not always be accompanied by WMA, particularly in non-ischemic heart disease, posing a significant challenge in detecting scars in such cases. To overcome this limitation, we propose a novel deep spatiotemporal residual attention network (ST-RAN) that leverages temporal and spatial information at different scales to detect scars in both ischemic and non-ischemic heart diseases. Our model comprises three primary components. First, we develop a novel factorized 4D (3D+time) convolutional layer that extracts 3D spatial features of the heart and a deep 1D kernel in the temporal direction to extract heart motion. Secondly, we enhance the power of the 4D (3D+time) layer with spatiotemporal attention to extract rich whole-heart features while tracking the long-range temporal relationship between the frames. Lastly, we introduce a residual attention block that extracts spatial and temporal features at different scales to obtain global and local motion features and to detect subtle changes in contrast related to scar. We train and validate our model on a large dataset of 3000 patients who underwent clinical CMR with various indications and different field strengths (1.5T, 3T) from multiple vendors (GE, Siemens) to demonstrate the generalizability and robustness of our model. We show that our model works on both ischemic and non-ischemic heart diseases outperforming state-of-the-art methods. Our code is available at https://github.com/HMS-CardiacMR/Myocardial_Scar_Detection.

Keywords: Contrast-Free MRI · Spatiotemporal Neural Network · 4D Convolution Factorization · Myocardial Scar Detection

H. Greenspan et al. (Eds.): MICCAI 2023, LNCS 14221, pp. 639–648, 2023.
https://doi.org/10.1007/978-3-031-43895-0_60

1 Introduction

Cardiovascular diseases continue to be the primary cause of death worldwide. Imaging of myocardial fibrosis/scar provides both diagnostic and prognostic information. Cardiac magnetic resonance (CMR) late gadolinium enhancement (LGE) is the gold standard for myocardial scar evaluation in ischemic and non-ischemic heart disease [7,8]. In LGE, imaging is performed 10–15 minutes after infusion of 0.1–0.2 mmol/kg of gadolinium-based contrast agent. However, many patients who undergo clinical CMR do not have any scars on LGE. While traditionally, gadolinium was considered safe; recent data show deposition of gadolinium in many organs, which is directly associated with the total dose of gadolinium [4,11,12]. Considering patients receiving multiple MRI scans throughout their life, it is important to minimize gadolinium use in imaging protocols with high field. Beyond patient safety, there is significant costs associated with gadolinium. Furthermore, concerns have arisen regarding environmental contamination due to excessive gadolinium use [5,15].

Recently, deep learning (DL) based methods have been proposed to limit gadolinium use by creating virtual LGE-like images using short-axis (sax) cine [22] or combined with native T_1 images [24]. The relationship between the motion field and myocardial infarction has also been explored to detect scar areas by learning temporal (dynamic) representations from cine images [20,21,23]. Another approach used radiomics alone [1,10,13] or combined with DL for myocardial scar screening [3]. Although promising, previous methods have several limitations. Changes in the mechanical properties of the myocardium caused by infarction can lead to regional wall motion abnormalities (WMA) [9]. However, WMA can occur in patients without scars [2]. Furthermore, the presence of scar may not always be accompanied by WMA, especially in non-ischemic heart disease [2], posing a significant challenge in detecting scars in such cases. The changes in contrast alone in cine images do not provide sufficient information to detect a scar [3]. Moreover, existing methods often overlook the 4D nature of the data (3D+time) and treat it as a 3D (2D+time) instead. Additionally, they require the detection of the left ventricle and were trained on 2D cine images that match LGE images, while in clinical practice, such information is not available beforehand. Finally, one of the major limitations is the lack of studies on large heterogeneous datasets [9].

Contribution: In this study, we develop a novel end-to-end deep spatiotemporal residual attention neural network (ST-RAN) for scar detection using whole heart imaging in ischemic and non-ischemic heart diseases. The proposed model leverages spatial information to capture changes in contrast and temporal information to capture WMA to detect scars, in a large heterogeneous dataset. To achieve this, we propose a novel efficient Conv3Plus1D layer that deploys a factorized 4D (3D+time) receptive field, to simultaneously extract hierarchical spatial features and deep temporal features (comprehensive spatiotemporal features), distinguishing between patients with and without a scar. We introduce a

multi-scale residual attention block that learns global and local motions to detect significant and subtle changes, the latter more present in patients with small scar sizes and nearly preserved wall motion. We validate our proposed model on a large cohort of patients with and without scars, showing the robustness of the model, outperforming state-of-the-art methods.

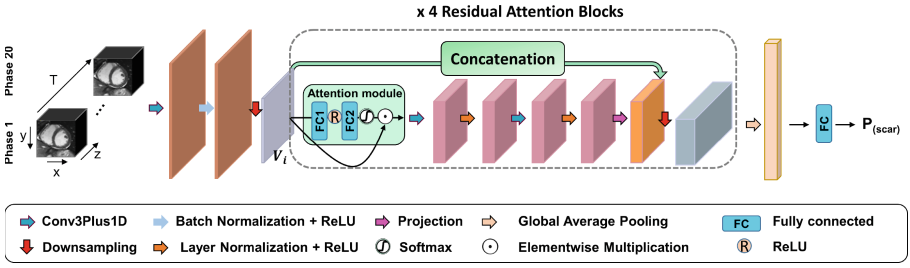

Fig. 1. Architecture overview. Our model takes an input a set of short-axis cine images of the whole heart, consisting of 20 phases, which are fed to a novel Conv3Plus1D layer, to extract spatial and temporal features. After batch normalization and non-linear transformation, the feature maps are fed to a series of residual attention blocks (RAB) at different scales to extract global and local features, subtle to changes due to myocardial scar. After the RAB, a global average pooling followed by a fully connected are used to predict presence of a scar.

2 Methods

As illustrated in Fig. 1, given a time series of a 3D volume of the heart, our goal is to predict the presence of a scar (Pscar). Inspired by recent work in image processing, we rely on residual attention network [18] to learn heart motion at different scales. In contrast to Zhang et al. [23] where they used a recurrent neural network to learn local motion features and an optical flow module to learn global motion features, our model enhances attention at different scales. This approach allows our model to capture local and global motion features within a single end-to-end network, reducing the complexity of using a two-stream model. The multi-scale temporal kernel allows to detect global motion, more likely to be related to a large scar size, and local motion to better estimate WMA at each segment. To address the heterogeneity of scar distribution, we have incorporated a spatiotemporal module to control the contribution of spatial features at different scales.

2.1 Spatiotemporal Decomposition Using 4D(3D+time) Layers

In sax cine, the data is in 4-dimension consisting of a 3D volume (stack of sax slices) with a temporal dimension. Therefore, effective representation of

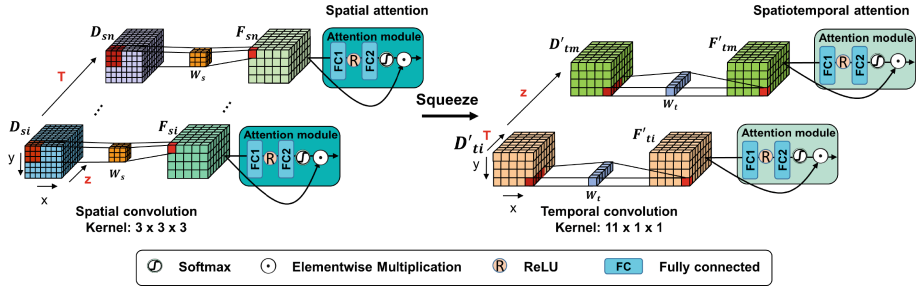

Fig. 2. Conv3Plus1D layer. The 4D convolution is factorized into a 3D spatial convolution to extract textural features, and a 1D temporal convolution to extract motion. Spatial attention helps in extracting meaningful features through the volume and spatiotemporal attention allows to maintain long range-dependency between the frames.

spatiotemporal features is crucial for accurate analysis. Inspired by Squeeze & Excitation network [6,14] and spatiotemporal network [17], we develop a novel efficient Conv3Plus1D layer that deploys a factorized 4D (3D+time) receptive field by applying a 3D spatial convolution of $3\times3\times3$ to extract hierarchical spatial features, followed by a 1D temporal convolution of $11\times1\times1$ to extract deep temporal features, as shown in Fig. 2. The large temporal filter allows maintain of the long-range dependency between the 20 frames. The input to the Conv3Plus1D layer is a 4D tensor $\mathcal{D} \in \mathbb{R}^{X\times Y\times Z\times T}$ where X is width, Y is high, Z is depth and T is time encoded in the channel-wise direction. The spatial convolution $\mathcal{W}_s$ is applied to input volume $\mathcal{D}_{si}$ across $X \times Y \times Z$ and its feature map output is $\mathcal{F}_{si} = W_s \times D_{si}$, where $i = 1....n$ and n is the number of feature maps in the T direction. The spatial attention module is trained to assign an attention score $\mathbf{a}_{fk}$ for each feature map F_{si}, and patch K in $X \times Y \times Z$ direction given as:

$$\mathbf{a}_{\mathrm{F_{si}k}} = \frac{e^{ReLU(\mathcal{F}_{si} * W_{c1}) * W_{c2}}}{\sum_{j=1}^{k} e^{ReLU(\mathcal{F}_{f|} * W_{c1}) * W_{c2}}} \tag{1}$$

where W_{c1} and W_{c2} are the weights for the fully connected layers 1 and 2 in the spatial attention module. The temporal convolution $\mathcal{W}_t$ is applied across a volume input $\mathcal{D}'_{ti}$ across $X \times Y \times T$ where the feature map output is $\mathcal{F}_{ti} = W_t \times D'_{ti}$, where $i = 1....m$ and m is the number of feature maps in the Z direction. The spatiotemporal attention module is trained to assign an attention score $\mathbf{a}_{F'k}$ for each feature map F_{ti} and patch K in $X \times Y \times T$ direction given as:

$$\mathbf{a}_{\mathrm{F'_{ti}k}} = \frac{e^{ReLU(\mathcal{F'}_{\mathrm{ti}} * W_{c3}) * W_{c4}}}{\sum_{j=1}^{k} e^{ReLU(\mathcal{F'}_{\mathrm{tj}} * W_{c3}) * W_{c4}}} \tag{2}$$

where W_{c3} and W_{c4} are the weights for the fully connected layers 1 and 2 in the spatiotemporal attention module.

To simplify the Eqs. (1) and (2), we have excluded the bias parameters. Following the application of softmax activation, the attention scores indicate the significance of each region in space and time, in determining the existence of a scar. Regions that are highly relevant to scar detection have scores near 1, while scar-free regions have scores near 0. Our proposed layer enables the learning of a more complete representation in spatial and temporal directions, surpassing a simple feature combination approach. Factorizing spatial and temporal kernels allows for reducing the model's parameters from 46M to 1.4M while learning rich spatiotemporal data representation.

2.2 Residual Attention Blocks

The motion patterns of the heart can evolve over time and scale. The residual attention network builds a stack of attention modules that generate attention-aware features. As the layers deepen, attention-aware features scale adaptively, enabling the detection of spatial and temporal subtle changes to be enhanced. This enhancement is crucial in accurately detecting small scar sizes. By aggregating information from tissues and motion across multiple scales, the attention module is able to learn and assign relative importance to each region with regard to the presence of a scar. The feature maps at a scale i where $i = 1....4$, are input to two fully-connected layers to encode spatial-wise and temporal-wise dependencies defined as $\mathcal{G} = W_{\text{Ri1}} * ReLU(V_i * W_{\text{Ri2}})$, with W_{Ri1} being the weights for the first fully connected layer at scale i, and W_{Ri2} being the weights for the second fully connected layer at scale i. The output $\mathcal{G}$ is then passed through the softmax activation to obtain the spatiotemporal residual weights, which will be applied to the input map V_i to extract the spatiotemporal features at scale i.

2.3 Network Details

The proposed network applies first a Conv3Plus1D layer followed by a batch normalization to mitigate internal covariate shift in the data, applies a small regularization effect, and a non-linear activation function ReLU. The output feature map is then resized through a customized resize frames layer that downsamples the size of the input by a factor of 2. This helps in increasing the batch size ($\times 2$ folds) and accelerates training ($\times 12$ folds) and testing ($\times 4$ folds) while maintaining the same high performance. This is followed by four attention residual blocks. Each block consists of residual attention applied to the input feature map and two sets of Conv3Plus1D layers, each followed by a layer normalization and ReLU. When layer normalization is located inside the residual blocks, it allows to speed-up convergence without a need for a learning rate warm-up stage [19]. Then a projection layer is applied to match the input data's last dimension and the residual block's output. When different-sized filters are used, and the input data is downsampled, the output may have a different number of filters than the input. The projection layer is used to project the last dimension of the input data to match the new filter size so that the input and output can be added together to form the residual connection. The concatenation helps tackle the vanishing

gradient problem due to the 4D nature of the input data with a large 3D volume and long-range temporal dependency. By using all these layers, the network can learn from the input data more effectively, handle different-sized inputs and outputs, and learn to recognize patterns in the temporal domain. Finally, to allow the model to learn scar-specific feature representations, a global 3D average pooling is applied to enforce correspondences between feature maps and the probability of a scar, the latter estimated through one fully connected neuron with a sigmoid.

3 Materials and Implementation Details

Data Aacquisition. Cine images were collected breath-hold electrocardiogram-gated balanced steady-state free precession sequence of 10 sax slices. The data were acquired from institution anonymous from 2016 to 2020 using multivendor (GE Healthcare, Siemens Healthineers) and different field strengths (1.5 T, 3 T). The institutional review board approved the use of CMR data for research with a consent waiver. Patient information was handled in compliance with the Health Insurance Portability and Accountability Act. Patients were referred for a clinical CMR for different cardiac indications, resulting in a heterogeneous patient cohort, necessary for better evaluation of the model performance. In total, 3000 patients (1697 males, 54 ± 18 years) were used for training and evaluation. The data were split into training (n=2000, 762 scar+), validation (n=500, 169 scar+), and testing (n=500, 199 scar+). All images were cropped at the center to a size of 128×128 and normalized to a fixed intensity range (from 0 to 1).

Implementation Details. The model's optimization was performed using a mini-batch stochastic gradient descent of 64 with an initial learning rate of 0.001 and a weight decay of 0.0001 when the validation loss plateaus. The model was trained for a maximum of 500 epochs with an early stopping of 70. The binary cross-entropy loss function and binary accuracy metric for both training and validation were monitored to avoid overfitting and underfitting. All models were implemented using TensorFlow version 2.4.1 and trained on an NVIDIA DGX-1 system equipped with 8 T V100 graphics processing units (each with 32 GB memory and 5120 cores). All selected hyperparameters were optimized experimentally. DeLong's test was used to compare the AUC of the different models. All tests were two-sided with a significance level = 0.05.

4 Experiments and Results

Ablation Study on the Impact of Different Components Design. We first perform an ablation study to evaluate each component's contribution to our proposed model. We test the effect of having spatial kernels only (S-CNN), temporal kernels only (T-CNN), and a combination of both (ST-CNN). We test the impact of spatial and temporal attention (AST-CNN) and residual attention (ST-RAN) on the performance of our network. To this end, we train five variants

Table 1. Effectiveness of different components of our proposed model (Ablation) and comparison with state-of-the-art methods (SOTA).

Study	Method	AUC	Sensitivity	Specificity	F_1-score	Nb. parameters
Ablation	S-CNN	0.74	0.74	0.60	0.63	0.90M
	T-CNN	0.81	0.77	0.70	0.70	0.38M
	ST-CNN	0.82	0.83	0.68	0.71	1.38M
	AST-CNN	0.83	0.79	**0.72**	0.71	1.42M
	ST-RAN	**0.84**	**0.90**	0.60	**0.72**	1.43M
SOTA	3D-STCNN [17]	0.77	0.84	0.52	0.66	0.44M
	3D-CNN [16]	0.80	0.81	**0.63**	0.68	46.5M
	CNN-LSTM [23]	0.79	0.81	0.59	0.67	0.33M
	ST-RAN	**0.84**	**0.90**	0.60	**0.72**	1.43M

of our model. We can observe from Table 1 that temporal information significantly outperforms spatial information alone (AUC= 0.81 vs. 0.74, $P = 0.004$). By combining both spatial and temporal information, we further increase the model's sensitivity (0.83 vs. 0.74, $P < 0.001$). Combining both spatial and temporal kernels with residual attention block yields the best performance on all dataset with an AUC of 0.84 and a sensitivity of 0.90. For both ischemic and non-ischemic heart diseases, ST-RAN showed higher sensitivity while having the lowest false-negative compared to others (Table 2).

Comparison with State-of-the-Art Methods. We then compare our model with state-of-the-art methods trained and tested on the same dataset for myocardial scar detection, including 3D (2D + time) spatiotemporal CNN (3D-STCNN) [17], 3D-CNN [16], and CNN with a long short-term memory network (CNN-LSTM) [23]. Our proposed model yields the best performance with a sensitivity of 0.90 and an F_1-score of 0.72, significantly outperforming all other methods (all $P < 0.05$), as shown in Table 1. We also compare different models on ischemic and non-ischemic patients, as shown in Table 2. We can notice the superiority of our model on both ischemic and non-ischemic patients outperforming other methods based on sensitivity, true positive, and false negative.

5 Discussion

Recent works using deep learning have shown the promise of contrast-free short-axis cine images to detect scars based on WMA in ischemic patients. However, these methods have limitations in detecting scar in non-ischemic heart diseases. Moreover, the large heterogeneous number of patients without scar in the dataset and with WMA has degraded these models' performance in detecting scar in ischemic patients. In contrast, our approach utilizes both spatial and temporal information to detect scar. Our model demonstrates superior performance over

Table 2. Ablation study and comparison with state-of-the-art methods for ischemic and non-ischemic heart diseases.

Study	Method	Sensitivity	True-positive	False-positive
Ischemic	S-CNN	0.74	79	28
	T-CNN	0.79	84	23
	ST-CNN	0.81	87	20
	AST-CNN	0.83	89	18
	3D-STCNN [17]	0.83	89	18
	3D-CNN [16]	0.82	88	19
	CNN-LSTM [23]	0.85	91	16
	ST-RAN	**0.92**	**98**	**9**
Non-Ischemic	S-CNN	0.74	68	24
	T-CNN	0.76	70	22
	ST-CNN	0.85	78	14
	AST-CNN	0.75	69	23
	3D-STCNN [17]	0.86	79	13
	3D-CNN [16]	0.79	73	19
	CNN-LSTM [23]	0.77	71	21
	ST-RAN	**0.89**	**82**	**10**

other methods in both ischemic and non-ischemic heart diseases. The inclusion of a multi-scale residual attention mechanism allows for the learning of global and local motions in an end-to-end network without the added complexity of a secondary component optical flow to extract global motion. Approximately half of non-ischemic cardiomyopathy patients who Gd-based imaging cardiac MRI exhibit no myocardial scars. Identifying these patients prior to Gd injection can significantly improve cost-effectiveness, scan efficiency, and safety by reducing unnecessary Gd administration.

To overcome the complexity of 4D convolution, we propose an effective training and inference strategy based on spatiotemporal factorization 4D (3D+time). This approach allows for a reduction in model parameters by a factor of 32 while maintaining high performance. The proposed layer extracts both spatial and temporal features, while enhancing attention on features in both directions, to detect subtle differences in left ventricle myocardial texture, as well as in cardiac motion.

In future work, we will investigate multimodality learning, incorporating other sequences such as T_1 maps, to enhance the model's precision to an even greater degree.

6 Conclusion

We propose a spatiotemporal residual attention neural network for myocardial scar detection, and we tackled the challenging non-ischemic patients. We showed that our model works on ischemic heart disease as well. Our results demonstrate the potential of our model in unmasking hidden information in native sax cine images, and allows for better detection of patients with a high likelihood of having a myocardial scar. These results indicate the potential of our proposed model in screening patients with and without a scar, thus, saving patients from unnecessary gadolinium based contrast agent administration, reducing costs, and environmental pollution. Finally, our proposed network has potential applications in various clinical contexts that require 4D processing.

References

1. Baessler, B., Mannil, M., Oebel, S., Maintz, D., Alkadhi, H., Manka, R.: Subacute and chronic left ventricular myocardial scar: accuracy of texture analysis on nonenhanced cine MR images. Radiology **286**(1), 103–112 (2018)
2. Csecs, I., et al.: Association between left ventricular mechanical deformation and myocardial fibrosis in Nonischemic cardiomyopathy. J. Am. Heart Assoc. **9**(19), e016797 (2020)
3. Fahmy, A.S., Rowin, E.J., Arafati, A., Al-Otaibi, T., Maron, M.S., Nezafat, R.: Radiomics and deep learning for myocardial scar screening in hypertrophic cardiomyopathy. J. Cardiovasc. Magn. Reson. **24**(1), 1–12 (2022)
4. Gulani, V., Calamante, F., Shellock, F.G., Kanal, E., Reeder, S.B., et al.: Gadolinium deposition in the brain: summary of evidence and recommendations. Lancet Neurol. **16**(7), 564–570 (2017)
5. Hatje, V., Bruland, K.W., Flegal, A.R.: Increases in anthropogenic gadolinium anomalies and rare earth element concentrations in san Francisco bay over a 20 year record. Environ. Sci. Technol. **50**(8), 4159–4168 (2016)
6. Hu, J., Shen, L., Sun, G.: Squeeze-and-excitation networks. In: Proceedings of the IEEE Conference on Computer Vision and Pattern Recognition, pp. 7132–7141 (2018)
7. Kim, R.J., et al.: Relationship of MRI delayed contrast enhancement to irreversible injury, infarct age, and contractile function. Circulation **100**(19), 1992–2002 (1999)
8. Kim, R.J., et al.: The use of contrast-enhanced magnetic resonance imaging to identify reversible myocardial dysfunction. N. Engl. J. Med. **343**(20), 1445–1453 (2000)
9. Leiner, T.: Deep learning for detection of myocardial scar tissue: Goodbye to gadolinium? (2019)
10. Mancio, J., et al.: Machine learning phenotyping of scarred myocardium from cine in hypertrophic cardiomyopathy. Eur. Heart J. Cardiovasc. Imaging **23**(4), 532–542 (2022)
11. McDonald, R.J., et al.: Gadolinium retention: a research roadmap from the 2018 NIH/ACR/RSNA workshop on gadolinium chelates. Radiology **289**(2), 517–534 (2018)
12. McDonald, R.J., et al.: Intracranial gadolinium deposition after contrast-enhanced MR imaging. Radiology **275**(3), 772–782 (2015)

13. Neisius, U., et al.: Texture signatures of native myocardial T1 as novel imaging markers for identification of hypertrophic cardiomyopathy patients without scar. J. Magn. Reson. Imaging **52**(3), 906–919 (2020)
14. Roy, A.G., Navab, N., Wachinger, C.: Concurrent spatial and channel 'Squeeze & Excitation' in fully convolutional networks. In: Frangi, A.F., Schnabel, J.A., Davatzikos, C., Alberola-López, C., Fichtinger, G. (eds.) MICCAI 2018. LNCS, vol. 11070, pp. 421–429. Springer, Cham (2018). https://doi.org/10.1007/978-3-030-00928-1_48
15. Schmidt, K., Bau, M., Merschel, G., Tepe, N.: Anthropogenic gadolinium in tap water and in tap water-based beverages from fast-food franchises in six major cities in Germany. Sci. Total Environ. **687**, 1401–1408 (2019)
16. Tran, D., Bourdev, L., Fergus, R., Torresani, L., Paluri, M.: Learning spatiotemporal features with 3d convolutional networks. In: Proceedings of the IEEE International Conference on Computer Vision, pp. 4489–4497 (2015)
17. Tran, D., Wang, H., Torresani, L., Ray, J., LeCun, Y., Paluri, M.: A closer look at spatiotemporal convolutions for action recognition. In: Proceedings of the IEEE Conference on Computer Vision and Pattern Recognition, pp. 6450–6459 (2018)
18. Wang, F., et al.: Residual attention network for image classification. In: Proceedings of the IEEE Conference on Computer Vision and Pattern Recognition, pp. 3156–3164 (2017)
19. Xiong, R., et al.: On layer normalization in the transformer architecture. In: International Conference on Machine Learning, pp. 10524–10533. PMLR (2020)
20. Xu, C., Howey, J., Ohorodnyk, P., Roth, M., Zhang, H., Li, S.: Segmentation and quantification of infarction without contrast agents via spatiotemporal generative adversarial learning. Med. Image Anal. **59**, 101568 (2020)
21. Xu, C., et al.: Direct detection of pixel-level myocardial infarction areas via a deep-learning algorithm. In: Descoteaux, M., Maier-Hein, L., Franz, A., Jannin, P., Collins, D.L., Duchesne, S. (eds.) MICCAI 2017. LNCS, vol. 10435, pp. 240–249. Springer, Cham (2017). https://doi.org/10.1007/978-3-319-66179-7_28
22. Xu, C., Xu, L., Ohorodnyk, P., Roth, M., Chen, B., Li, S.: Contrast agent-free synthesis and segmentation of ischemic heart disease images using progressive sequential causal gans. Med. Image Anal. **62**, 101668 (2020)
23. Zhang, N., et al.: Deep learning for diagnosis of chronic myocardial infarction on nonenhanced cardiac cine MRI. Radiology **291**(3), 606–617 (2019)
24. Zhang, Q., et al.: Toward replacing late gadolinium enhancement with artificial intelligence virtual native enhancement for gadolinium-free cardiovascular magnetic resonance tissue characterization in hypertrophic cardiomyopathy. Circulation **144**(8), 589–599 (2021)